

Application note

# Mechanical properties of bioprinted hydrogels

May, 2025 For Research Use Only.

## Unlock greater mechanical property insights on bioprinted constructs via nanoindentation

by Elizaveta Loseva<sup>1</sup>, Massimiliano Berardi<sup>1</sup>, Elin Pernevik<sup>2</sup>, Volodymyr Kuzmenko<sup>2</sup>, Avijit K Minocha<sup>2</sup>

<sup>1</sup> Optics11 Life, Amsterdam, the Netherlands

<sup>2</sup> CELLINK Bioprinting AB, Gothenburg, Sweden

© 2025 Optics11 Life B.V.

Bioprinted hydrogel structures provide a practical strategy for replicating environmental cues in cellular *in vitro* studies. Despite advances in bioprinting technologies and biomaterial development, creating truly biomimetic models can still be challenging. The mechanical properties of bioprinted constructs play a key role in effectively recapitulating native environments, as they affect cell behavior and overall tissue function.

In this application note, we highlight how commercially available bioprinters, like the BIO X6 from CELLINK, can be combined with Pavone, Optics11 Life's high-throughput nanoindenter, to successfully develop physiologically relevant constructs, and provide a workflow for capturing critical information around the mechanical properties, to further streamline hydrogel testing and model optimization.



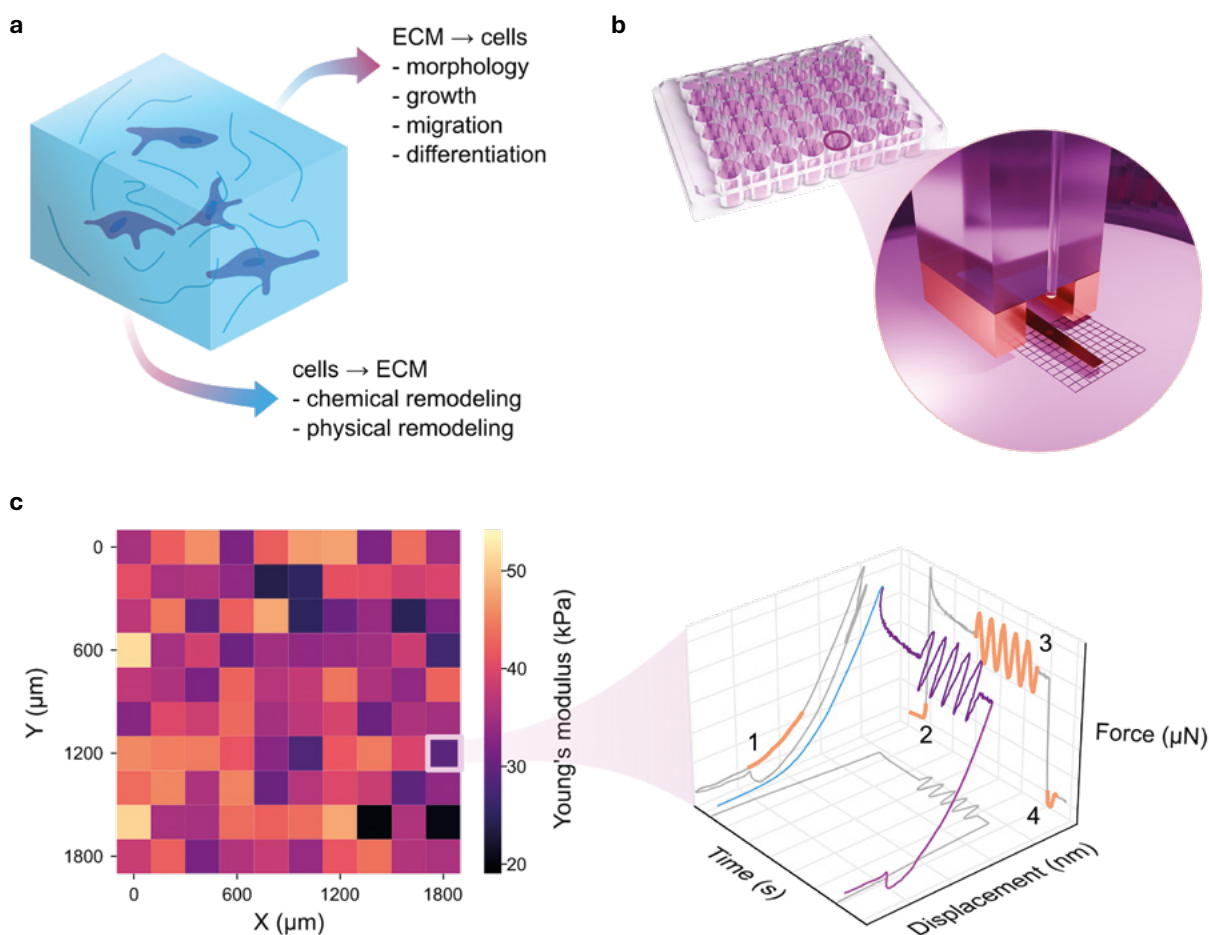
# Introduction

Cellular behavior is dictated by its microenvironment – a combination of soluble and immobilized signaling molecules, matrix composition and architecture, as well as physical properties<sup>1</sup>.

Amongst the latter, viscoelastic properties are particularly interesting. This is because local variations in matrix elasticity or viscosity have been shown to direct physiological cellular behavior<sup>2</sup>, as well as to play a role in the progression of pathological conditions<sup>3</sup>. For example, variations in substrate stiffness can induce fibroblast activation which,

in turn, leads to microenvironment remodeling in the form of extracellular matrix (ECM) deposition<sup>4</sup>. In Figure 1-a, a schematic summary of the interplay between cells and their environment is shown.

Given the advancements and increase in access of bioprinters and bioinks, bioprinted *in vitro* models can and should integrate this knowledge<sup>5</sup>, with particular care put into the replication of mechanical cues at the cell scale<sup>6</sup>. The incorporation of this essential element is instrumental to the biofabrication of advanced *in vitro* models that can acceler-



▲ **Figure 1**

Overview of cell-ECM reciprocal interactions and of Pavone nanoindentation technology. **(a)** Schematic depiction of how ECM mechanics instructs cellular behavior, providing adhesive cues and durotactic gradients, as well as how cells affect ECM, in terms of generation of contractile forces, crosslinking, matrix degradation and deposition. **(b)** Illustration of Pavone's force sensor measuring within a 48-well plate, highlighting how mechanical properties can be mapped in space. **(c)** Example of data output from a nanoindentation assay. Each pixel corresponds to a mechanical spectrum (callout to the right). This load-displacement data in time can be used to extrapolate 1) elastic modulus, 2) sample topography, 3) viscoelastic and 4) adhesive properties, as highlighted in the data projections.

ate insights within cell biology applications. Combining the right biomaterials<sup>7,8</sup>, either natural or synthetic, with the appropriate printing conditions provides a practical mean to this end. However, the wide variation in viscoelastic properties across different organs, tissues, and physiological conditions<sup>9</sup> poses a challenge in creating matrices suitable for the model of interest. On top of that, the need to explore a large parameter space in terms of gel compositions and manufacturing routes makes the search for optimal biomimetic systems difficult and resource-intensive<sup>10</sup>.

This highlights the need for (i) biomaterials with highly tunable mechanical characteristics, (ii) an effective method to print these materials and (iii) a scalable mechanical characterization method, such as nanoindentation, to provide qualitative and quantitative feedback on the mechanical properties of the printed constructs. Combining CELLINK's BIO X6 extrusion based bioprinter and associated bioinks with Optics11 Life's Pavone provides an intuitive and effective workflow that addresses these unmet needs.

Pavone is a mechanical screening platform that integrates mechanical testing and microscopy. It can perform quasi-static mechanical testing, in control of displacement, strain rate, stress rate, as well as dynamic mechanical analysis. Its ability to autonomously engage samples, move from condition to condition, correlate mechanics and microscopy, and spatially map properties makes it an ideal solution for large scale testing of biomaterials. Thanks to a unique sensor design, it enables the measurement of mechanical properties within most common labware. In Figure 1-b/c, we show an illustration of a measurement and data output, in the form of a Young's modulus heatmap. Pavone collects force-distance curves (see magnified view on the right), which can be used to extract many

more parameters, such as sample topography, viscoelastic and adhesive properties.

In this work, we exploit Pavone's ability for multi-parametric characterization of various CELLINK hydrogels, in cast and printed form, demonstrating how mechanical properties can be tuned both through material design, as well as through construct design and printing parameters on the BIO X6 bioprinter. We show how these technologies can be combined to unlock greater understanding around hydrogels, enable better material selection, validate engineered scaffolds, as well as perform functional studies on 3D *in vitro* models.

## Results and Discussion

First, we evaluated the effect of different material parameters, such as ion concentration and chemical crosslinking density on cast hydrogel samples. Figures 2 and 3 summarize the results of the mechanical screening performed on two hydrogels, differing by composition: (1) CELLINK Bioink, composed of nanocellulose and alginate, ionically crosslinked with 50 mM  $\text{CaCl}_2$  and (2) GelMA Bioink, composed of gelatin methacrylate (GelMA) and crosslinked via near-UV exposure using LAP as a photoinitiator.

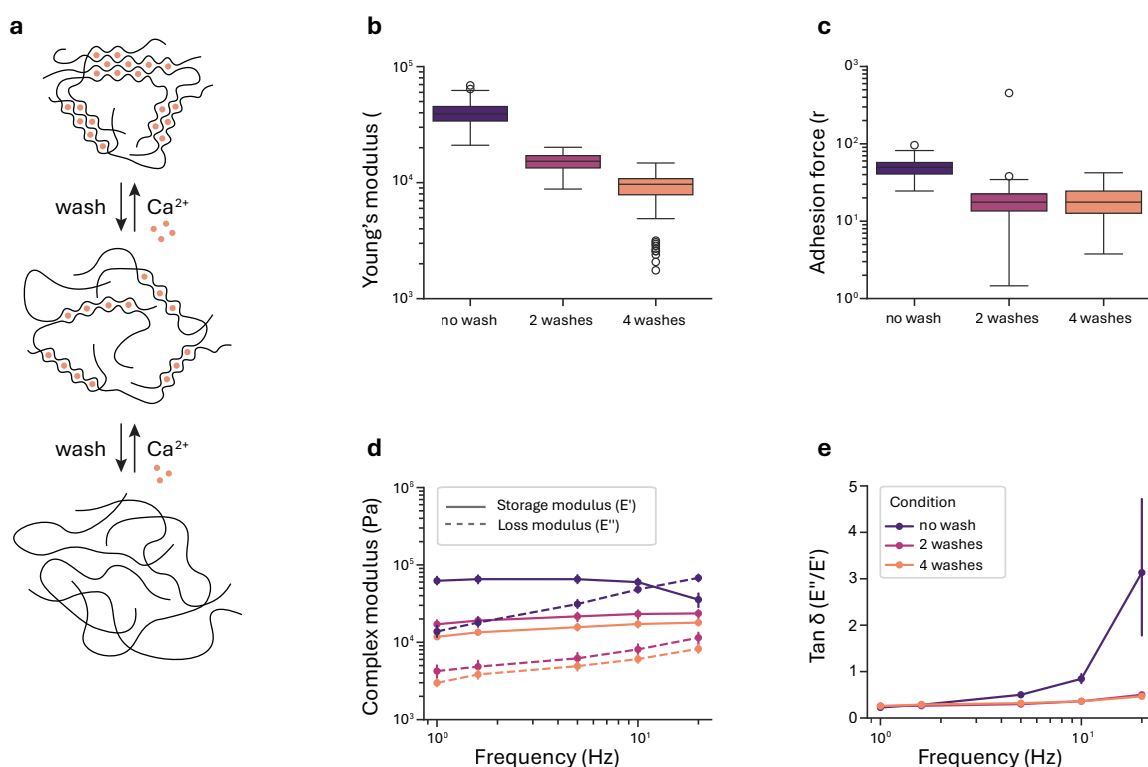
In the case of ionically crosslinked CELLINK Bioink (Figure 2), we can see how progressive washes lead to a successive decrease in Young's modulus from 40 to 10 kPa (Figure 2-b) over the course of four washes (corresponding to cell media or buffer exchanges). This is due to the progressively lower concentration of  $\text{Ca}^{2+}$  ions in the surrounding environment and the consequent weaker interaction between polymer chains. We see a similar reduction in adhesive properties (from 50 to 15 nN; Figure 2-c), which, unlike the Young's modulus, plateaus after the first wash, most likely

due to a more rapid exchange of ions on the surface of the sample. Dynamic mechanical analysis (DMA, Figure 2-d) results are aligned with the quasi-static screening but provide further insight into the rheological behavior of the hydrogel: the “no wash” condition appears the stiffest, and in all conditions the storage modulus remains relatively stable in the tested range, whilst viscous losses increase log-linearly with frequency. As the number of washes increases, the complex modulus curves shift towards lower values. However, the shift is not rigid: whilst the “no wash” condition features a low frequency  $\tan \delta$  of  $\sim 0.25$  (i.e. the ratio of viscous losses to elastically stored energy) that matches the other conditions, it has a much steeper dependency on frequency, resulting in a solid-liquid transition at  $\sim 15$  Hz (Figure 2-e).

In the case of photocrosslinked GelMA (Figure 3), we see the effect of progressively longer near-UV light exposure times on mechanical properties. As

the time increases from 5 to 30 s, Young’s modulus increases greatly, from 300 Pa to 4 kPa (Figure 3-b). Simultaneously, adhesive properties decrease marginally. The median adhesion plateaus after 15 s of exposure, though it is possible to qualitatively observe an additional effect at 30 s of exposure in the form of a distribution with a longer tail towards lower adhesion values (Figure 3-c).

DMA results confirm the light exposure-dependent stiffening. Similarly to the case of ionically cross-linked hydrogels, the storage moduli remain constant in the tested range, whilst viscous losses are weakly dependent on actuation frequency (Figure 3-d). The  $\tan \delta$  vs frequency plot shows how, as the degree of crosslinking increases, the hydrogels behave more and more as purely elastic systems irrespective of the tested frequency. For example, viscous losses measured at 5 Hz drop 5-fold between 5 and 30 seconds of light exposure (from 0.25 to  $\sim 0.05$ , Figure 3-e).



▲ **Figure 2**

Summary of the nanoindentation assay on ionically crosslinked cast CELLINK hydrogels. (a) Schematic representation of the crosslinking process and effect of washing for CELLINK Bioink. Dependency of Young’s modulus (b), adhesion force (c), complex modulus (d) and  $\tan \delta$  (e) on washing of samples.

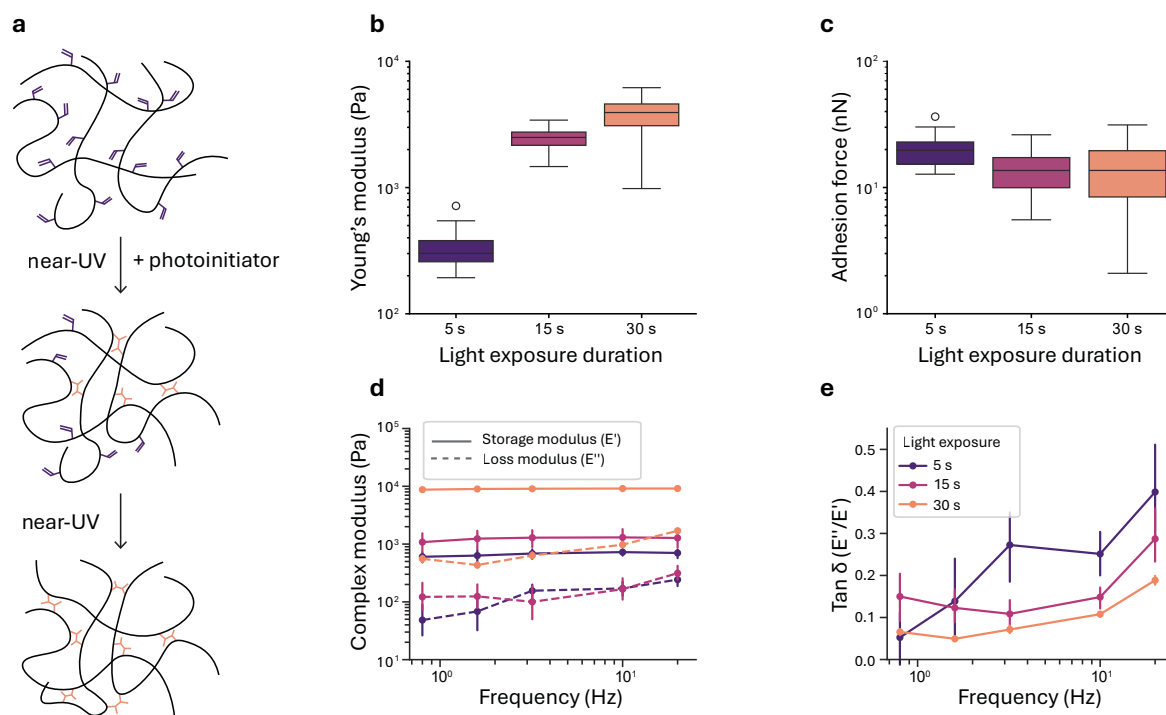


**Figure 3**

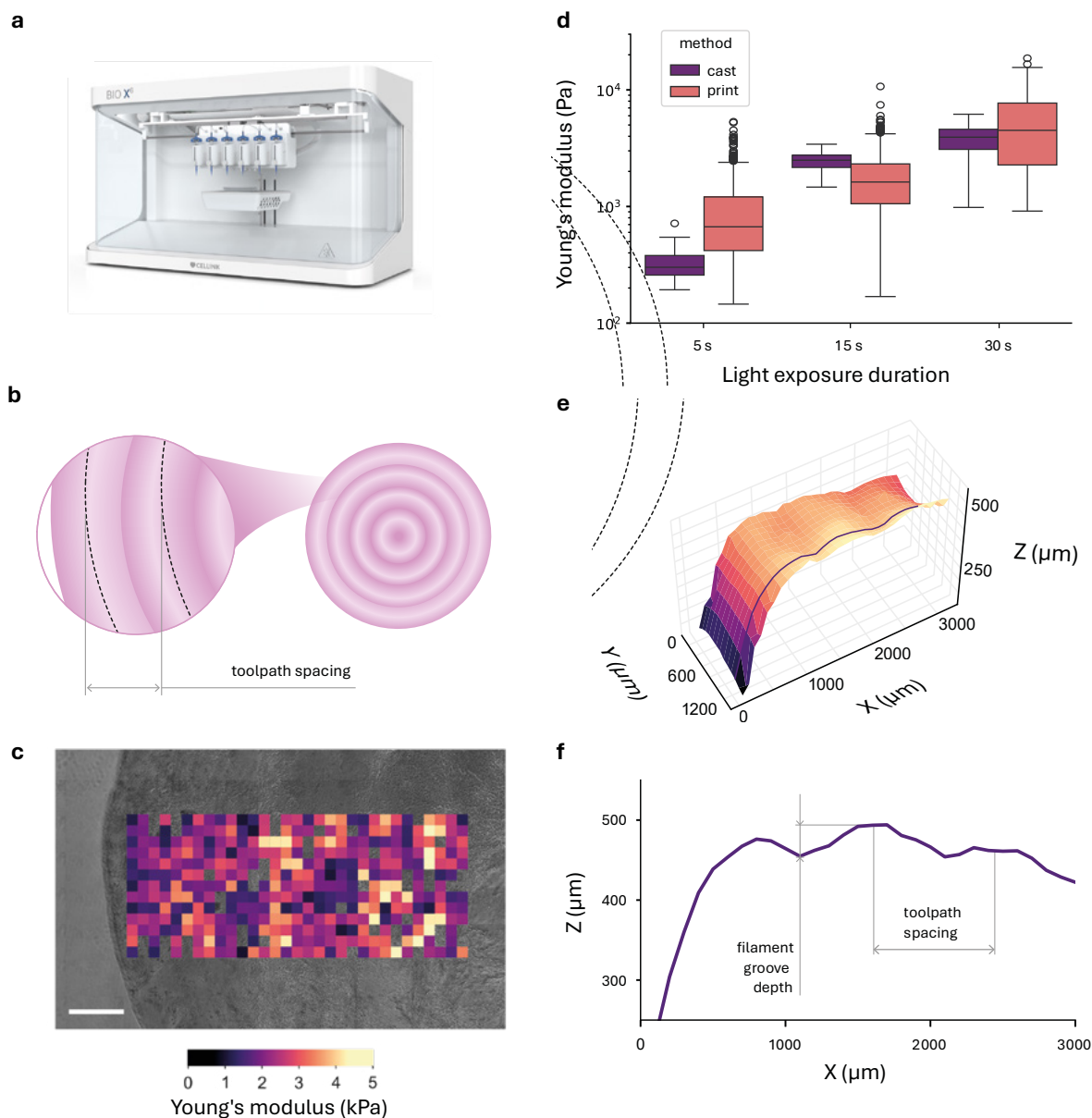
Summary of the nanoindentation assay on cast photocrosslinked GelMA Bioink from CELLINK. **(a)** Schematic representation of the crosslinking process for GelMA Bioink from CELLINK. Dependency of Young's modulus **(b)**, adhesion force **(c)**, complex modulus **(d)** and  $\tan \delta$  **(e)** on light exposure duration.

Once a specific hydrogel chemistry and a set of desired physical properties are chosen, it is important to also validate the final product, for example a scaffold to be used for an *in vitro* study. This is because the manufacturing route can impact final properties, e.g. in the form of polymer chain alignment during an extrusion process compared to casting<sup>11</sup>. In Figure 4 we show a simple example of such an application: using a BIO X6 bioprinter (Figure 4-a), we printed a set of GelMA disks composed of concentric rings on a 48-well plate. We then used the Pavone to image them in brightfield and to map morphology and elastic properties.

In Figure 4-b, is a schematic representation of the printed disk under study, with the callout highlighting some of the print parameters. The result of the mechanical assay with Pavone is shown in Figure 4-c/f: after imaging a portion of the printed

disk, we mapped a region spanning across the concentric circles, to observe the distribution of the Young's modulus as a function of position within the print (Figure 4-c).

The trends of Young's moduli as a function of near-UV exposure are preserved (Figure 4-d), although the distribution of moduli values of printed structures appear broader, with the first printed condition also being stiffer than its cast counterpart. Part of the increased variability can be ascribed to the varying substrate angle with respect to the indenter head but is also partially owed to the more complex manufacturing process. Moreover, polymer chain alignment during extrusion may have a more pronounced effect on weakly crosslinked bioinks, as suggested by the printed GelMA Bioink photocrosslinked for 5 s. This effect appears to be progressively masked as the mechanical response becomes dominated by



▲ **Figure 4**

*Nanoindentation assay performed on 3D printed structures. (a) The BIO X6 3D printer was used to manufacture the disks. (b) Schematics of the printed disk. (c) Overlay of microscopy and mechanical imaging obtained with the Pavone. Scale bar 500  $\mu\text{m}$ . (d) Comparison between the Young's modulus distribution of photocrosslinked GelMA when cast in a well plate or deposited via the BIO X6. (e) Reconstruction of the 3D surface of the print. (f) Detail of the printed disk topography, highlighting some of the print features.*

the crosslinked network rather than by secondary interactions between polymer chains.

An interesting aspect of this correlative measurement is that it enables the use of topographical data to verify and potentially inform the printing process. In Figure 4-e, we show a 3D plot of the sample topography, from which it is possible to

see the printed filaments. Figure 4-f shows one of the scan lines, highlighting the consistency of filaments' center-to-center distance, as well as the rather negligible height variation between the concentric circles.

# Conclusions

- Nanoindentation streamlines analysis of large material libraries to find optimal compositions for given *in vitro* applications.
- Hydrogels from CELLINK provide a great degree of tunability in terms of viscoelastic behavior and adhesive properties.
- Nanoindentation can be used to assess the quality of printed constructs, in terms of both distribution of mechanical properties and morphology, providing quantitative metrics that can help fine-tune the manufacturing parameters.
- Utilizing existing solutions from CELLINK and Optics11 Life, an intuitive workflow combining extrusion printing with nanoindentation can be carried out. This workflow gives comprehensive insight into the mechanical properties of biofabricated constructs, allowing for greater mechanical tuning and subsequent development of physiologically relevant *in vitro* models.
- The label-free and non-destructive nature of the mechanical characterization makes it possible to perform measurements on gels or printed constructs populated with cells, expanding the measurements presented here to possible longitudinal studies.

## Materials and Methods

### Bioinks

CELLINK Bioink contains nanocellulose and alginate that allows ionic crosslinking with divalent cations such as  $\text{Ca}^{2+}$ .

GelMA Bioink contains 10% (w/v) gelatin (of porcine origin) methacrylate at 45-65 degrees of methacrylation (DoM), with 0.25% lithium phenyl-2,4,6-trimethylbenzoylphosphinate (LAP) photoinitiator, and can be photocrosslinked using 405 nm light, among other wavelengths.

### Casting of bioink samples

A 10-100  $\mu\text{l}$  positive-displacement pipet was used to dispense 80  $\mu\text{l}$  of bioink samples into 48-well plates. GelMA was pre-warmed for 30 min at 37°C before loading to ensure a low viscosity melt that would distribute evenly over the well's surface. CELLINK Bioink, which does not have a temperature-dependent viscosity, was directly pipetted into the wells. Both plates were immediately centrifuged for 2 min at 180 rcf to help form an even gel layer in each well.

## 3D printing of bioink samples

The BIO X6 was used to 3D print 8-mm disks into 24-well plates, with the 20 g (580  $\mu\text{m}$ ) nozzle size selected to create wide filament ridges and concentric infill of 50%, without perimeter. The G-code for the disks of 8 mm diameter and 0.6 mm height was created in DNA Studio.

GelMA was pre-warmed for 30 min at 37°C before being loaded into the temperature-controlled printhead for 10 min of equilibration at 27°C. A temperature slightly above recommended printing temperature was chosen to maintain a lower viscosity allowing some merging of printed filaments as height difference above 150  $\mu\text{m}$  between peak and groove could cause challenges for the nanoindentation probe. Printbed temperature was 23°C also to allow for some merging of filaments. Print settings were: 16 kPa extrusion pressure, -100 ms preflow (pressure started before movement, 10 mm/s translational speed).

## Crosslinking of cast and printed samples

The cast and printed bioink samples were cross-linked using the same procedures. Ionic crosslinking was performed by addition of  $\text{CaCl}_2$  Crosslinking Agent (50 mM): 200  $\mu\text{l}$  to the cast samples in 48-well plates and 500  $\mu\text{l}$  to the printed samples in 24-well plates. To simulate the ion concentrations of cell culture over time, some ionically crosslinked bioinks were washed for 10 min in HBSS, followed by 2 media changes with 2 h time separation, specifically DMEM containing 1.8 mM  $\text{CaCl}_2$  was used as a medium, supplemented with 5% Antibiotic Antimycotic (anti-anti). Photocrosslinking of GelMA was performed with the BIO X6 built-in 405 nm LED module. The plates were placed in the printbed at ambient temperature (23°C) and photocrosslinked at 5 cm distance (corresponding to 43  $\text{mW}/\text{cm}^2$  irradiance) for 5-30 s. Photocross-

linked samples were directly immersed in media. All wells were filled to the brim with either ionic crosslinking agent or media and covered with PCR film for shipment to Optics11 Life.

## Nanoindentation assay

We performed the mechanical characterization of hydrogels and printed constructs with a Pavone nanoindenter, paired with probes with cantilever stiffness  $k$  between 0.44 and 0.5 N/m, and tip radii between 25 and 49.5  $\mu\text{m}$ . We used the probe with the smaller tip in the case of printed sample, to extract a more accurate topography, with a less pronounced tip-sample convolution error.

We used three different data collection protocols, depending on the experiment:

1. When investigating elastic and adhesive properties of cast samples we collected 10x10 matrices, with points separated by 200  $\mu\text{m}$  in both X and Y directions, for a total area coverage of  $\sim 4 \text{ mm}^2$  around the center of each well. We used peak load poking (PLP) as a probing method, with a piezo speed of 30  $\mu\text{m}/\text{s}$  and a peak load tuned to each sample, so that the resulting indentation would fall between 5 and 10  $\mu\text{m}$ .
2. When investigating viscoelastic behavior, we collected 4x4 matrices, with points separated by 400  $\mu\text{m}$  in both X and Y directions, for a total area coverage of  $\sim 2.6 \text{ mm}^2$  around the center of each well. We used dynamic mechanical analysis (DMA) as a probing method, setting target indentation depth between 3 and 5  $\mu\text{m}$ , and 200 nm oscillating amplitude between 1 and 20 Hz.
3. When investigating 3D printed samples, we first acquired an image stitch of the printed construct within each well. Then, we defined an area of interest spanning over the printed concentric cir-

cles and defined an overlaying scan. This was typically 3x2 mm, with points separated by 100  $\mu\text{m}$  in both X and Y direction. We used PLP as a probing method, with a piezo speed of 30  $\mu\text{m/s}$  and a peak load tuned to each sample, so that the resulting indentation would fall between 2 and 5  $\mu\text{m}$ .

We performed all experiments with samples immersed in their media, with temperature control set at 37°C. In every test, plates were let acclimatize for about 4 hours before the start of the measurements. In the case of printed samples, we enabled “adaptive surface” mode, where the probe stage automatically adjusts its position to hover conformally to irregularly shaped samples.

We obtained mechanical properties using Optics11 Life analysis software. To extract the elastic modulus, we used the Hertz model. We either limited the fit to 2 or 4  $\mu\text{m}$  of indentation depth (depending on the tip radius). To extract adhesive properties, we use the JKR model, setting  $P_{\text{max}}$  between 50 and 80% depending on the sample.

In all cases, we rejected data based on fit R2 (>0.95 for quasi-static testing, >0.5/0.7 for adhesion characterization), removed curves starting in contact and curves that the software classified as not suitable to be modeled.

## References

- 1 **Young, J. L., Holle, A. W. & Spatz, J. P.** Nanoscale and mechanical properties of the physiological cell–ECM microenvironment. *Exp. Cell Res.* 343, 3–6 (2016).
- 2 **Kamperman, T. et al.** Steering Stem Cell Fate within 3D Living Composite Tissues Using Stimuli-Responsive Cell-Adhesive Micromaterials. *Adv. Sci.* 10, 2205487 (2023).
- 3 **Fan, W. et al.** Matrix viscoelasticity promotes liver cancer progression in the pre-cirrhotic liver. *Nature* 626, 635–642 (2024).
- 4 **Petersen, A., Joly, P., Bergmann, C., Korus, G. & Duda, G. N.** The Impact of Substrate Stiffness and Mechanical Loading on Fibroblast-Induced Scaffold Remodeling. *Tissue Eng. Part A* 18, 1804–1817 (2012).
- 5 **Holle, A. W. et al.** Cell–Extracellular Matrix Mechanobiology: Forceful Tools and Emerging Needs for Basic and Translational Research. *Nano Lett.* 18, 1–8 (2018).
- 6 **Ciccione, G. et al.** What Caging Force Cells Feel in 3D Hydrogels: A Rheological Perspective. *Adv. Healthc. Mater.* 9, 2000517 (2020).
- 7 **Fu, X. et al.** Targeting Nuclear Mechanics Mitigates the Fibroblast Invasiveness in Pathological Dermal Scars Induced by Matrix Stiffening. *Adv. Sci.* 11, 2308253 (2024).
- 8 **Blache, U. et al.** Engineered hydrogels for mechanobiology. *Nat. Rev. Methods Primers* 2, 98 (2022).
- 9 **Singh, G. & Chanda, A.** Mechanical properties of whole-body soft human tissues: a review. *Biomed. Mater.* 16, 062004 (2021).
- 10 **Yang, L. et al.** High-Throughput Methods in the Discovery and Study of Biomaterials and Materiobiology. *Chem. Rev.* 121, 4561–4677 (2021).
- 11 **Christensen, K., Davis, B., Jin, Y. & Huang, Y.** Effects of printing-induced interfaces on localized strain within 3D printed hydrogel structures. *Mater. Sci. Eng. C* 89, 65–74 (2018).

OPTICS11life

CELLINK  
A BICO COMPANY



[www.optics11life.com](http://www.optics11life.com)